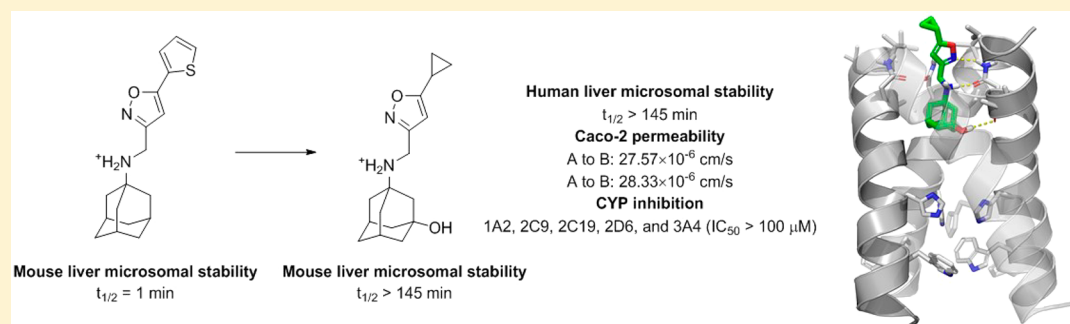


In Vitro Pharmacokinetic Optimizations of AM2-S31N Channel Blockers Led to the Discovery of Slow-Binding Inhibitors with Potent Antiviral Activity against Drug-Resistant Influenza A Viruses

Yuanxiang Wang,^{†,⊥} Yanmei Hu,^{†,⊥} Shuting Xu,[†] Yongtao Zhang,[†] Rami Musharrafieh,[‡] Raymond Kin Hau,[†] Chunlong Ma,[§] and Jun Wang^{*,†,§}[†]Department of Pharmacology and Toxicology, College of Pharmacy, The University of Arizona, Tucson, Arizona 85721, United States[‡]Department of Chemistry and Biochemistry, The University of Arizona, Tucson, Arizona 85721, United States[§]BIOS Institute, The University of Arizona, Tucson, Arizona 85721, United States

Supporting Information



ABSTRACT: Influenza viruses are respiratory pathogens that are responsible for both seasonal influenza epidemics and occasional influenza pandemics. The narrow therapeutic window of oseltamivir, coupled with the emergence of drug resistance, calls for the next-generation of antivirals. With our continuous interest in developing AM2-S31N inhibitors as oral influenza antivirals, we report here the progress of optimizing the in vitro pharmacokinetic (PK) properties of AM2-S31N inhibitors. Several AM2-S31N inhibitors, including compound **10b**, were discovered to have potent channel blockage, single to submicromolar antiviral activity, and favorable in vitro PK properties. The antiviral efficacy of compound **10b** was also synergistic with oseltamivir carboxylate. Interestingly, binding kinetic studies (K_d , K_{on} , and K_{off}) revealed several AM2-S31N inhibitors that have similar K_d values but significantly different K_{on} and K_{off} values. Overall, this study identified a potent lead compound (**10b**) with improved in vitro PK properties that is suitable for the in vivo mouse model studies.

INTRODUCTION

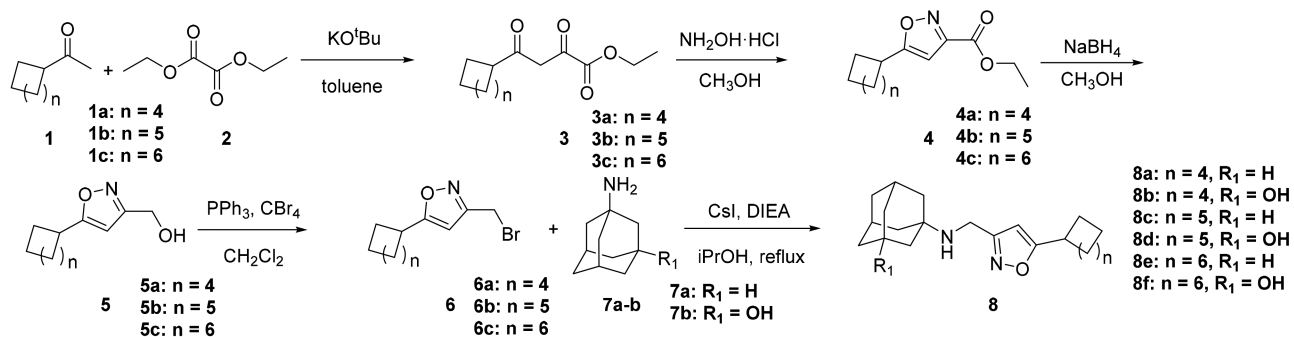
Influenza viruses are respiratory pathogens that are responsible for both seasonal influenza epidemics and sporadic influenza pandemics.¹ Influenza A and B viruses co-circulate among humans in each influenza season; however, the strains and ratios change over time, and it is often difficult to predict which strains will be circulating in the next influenza season and when the next influenza pandemic will emerge.² In addition, the mortality rates for different subtypes of influenza viruses vary significantly. For example, the mortality rates for human infections with avian H5N1 and H7N9 viruses are 52.7% and 38.6%, respectively (WHO), compared to the 0.1–2.5% mortality rate associated with past H1N1 influenza pandemic viruses.^{3,4} Moreover, people in the high-risk groups of influenza virus-related complications are more vulnerable for influenza virus infection than immune-competent adults.⁵ Therefore, effective antiviral drugs are undoubtedly needed for the prevention and treatment of influenza virus infection.⁶

There are two classes of FDA-approved influenza antivirals: M2 channel blockers (amantadine and rimantadine),⁷ and neuraminidase inhibitors (oseltamivir, zanamivir, and peramivir).⁸ Amantadine and rimantadine are no longer recommended by the CDC for the prevention and treatment of influenza virus infection due to the prevalent drug resistance.⁹ Oseltamivir is currently the only FDA-approved oral influenza drug. Zanamivir is administered through intranasal spray; therefore, its use is limited in infants and critically ill patients. Recently approved peramivir is an intravenous drug and its use is restricted in clinical settings. Although a majority of current circulating influenza viruses remain sensitive to oseltamivir, oseltamivir-resistant viruses have been continuously reported,^{10,11} and more alarmingly, the 2007–2008 seasonal influenza H1N1 strain circulating in North America and Japan

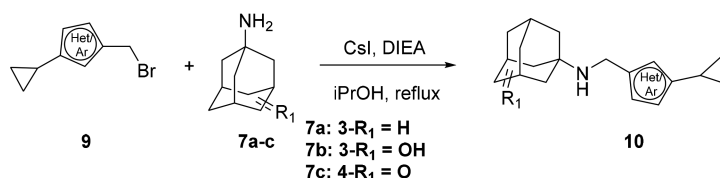
Received: October 14, 2017

Scheme 1. Synthesis of AM2-S31N Inhibitors

A. Synthesis of isoxazole-containing AM2-S31N inhibitors



B. Direct alkylation



was completely resistant to oseltamivir due to the H275Y mutation in the neuraminidase gene.^{12,13} In this regard, the next generation of oral influenza drugs with a novel mechanism of action is clearly needed.

More than 95% of current circulating influenza A viruses carry the AM2-S31N mutant in their AM2 genes,¹⁴ which confer to amantadine and rimantadine resistance. Given the high prevalence of the AM2-S31N mutant, we hypothesize that AM2-S31N inhibitors will have potent antiviral activity against both oseltamivir-sensitive and -resistant influenza A strains. Indeed, we have shown that our rationally designed AM2-S31N inhibitors inhibit multiple human influenza A viruses with submicromolar efficacy, including oseltamivir-resistant strains.^{15–18} Encouraged by these preliminary results, in this study, we report our progress in optimizing the *in vitro* PK properties of AM2-S31N inhibitors with the aim of prioritizing lead compounds for the next step *in vivo* mice studies. Through iterative cycles of hypothesis-driven PK optimization, we identified one compound, **10b**, with optimal *in vitro* PK properties. Interestingly, unlike most other previously reported AM2-S31N inhibitors which have fast K_{on} and slow K_{off} values, compound **10b** is a slow binding channel blocker with slow K_{on} and K_{off} values but having a low micromolar K_d . Subsequent kinetic studies of several representative AM2-S31N inhibitors revealed that the antiviral efficacy of AM2-S31N inhibitors has a better correlation with their K_d values rather than their percentage of channel blockage at the 2 min time point.

RESULTS AND DISCUSSION

Chemistry. Compounds **8a–8f** were synthesized according to a previous optimized synthesis route (Scheme 1A).¹⁸ Briefly, condensation of methyl ketone **1** and diethyl oxalate **2** using potassium *tert*-butoxide as the base gave the β -ketone ester intermediate **3**, which was cyclized to isoxazole ester **4** by heating at 50 °C in methanol with hydroxylamine hydrochloride. The ester **4** was reduced to alcohol **5** by sodium borohydride and was then converted to bromide **6** by triphenyl phosphine and carbon tetrabromide in dichloromethane. Last, alkylation of bromide **6** with the amantadine analogue **7** gave

the isoxazole-containing AM2-S31N inhibitor **8**. The overall yields range from 15% to 36%. Compounds **10a–10g** were synthesized by direct alkylation (Scheme 1B). The yields range from 62% to 85%. The synthesis of compounds **11**, **14**, **15**, and **16** was reported before.^{16,18,19}

Hypothesis-Driven Optimization of the *in Vitro* PK Properties Of AM2-S31N Inhibitors. The lead optimization was guided by the solution NMR structure of compound **11** in complex with AM2-S31N (19–49) (PDB 2LY0) (Figure 1).¹⁹ Compound **11** binds to the central cavity of the AM2-S31N channel with its aryl group projecting toward the N-terminal channel lumen. The distal thiophene substitution from compound **11** forms hydrophobic interactions with V27 side chain methyls, the isoxazole and the amine form bidentate

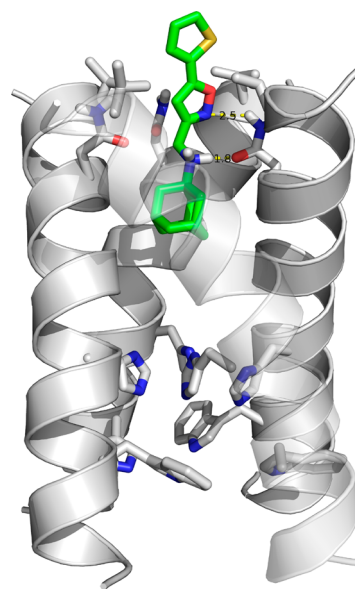
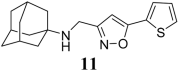
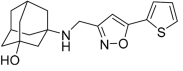
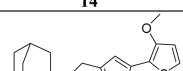
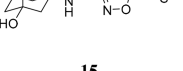
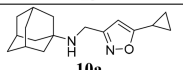
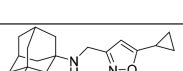
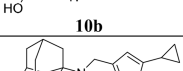
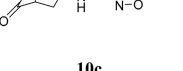
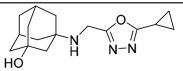
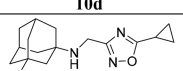
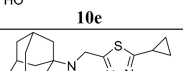
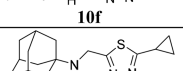
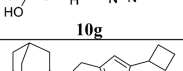
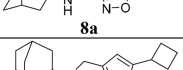
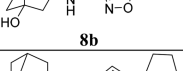
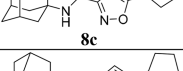


Figure 1. Solution NMR structure of compound **11** in complex with the transmembrane domain of AM2-S31N (PDB 2LY0).¹⁹ The transparency of the front helix was set as 0.5 for clarity.

Table 1. Channel Blockage, Antiviral Efficacy, Cytotoxicity, and Mouse Microsomal Stability of AM2-S31N Inhibitors

Structure/Compound ID	Electrophysiological TEVC assay ^a (% S31N channel inhibition)	Electrophysiological TEVC assay ^a (% WT channel inhibition)	EC ₅₀ (μM) A/California/07/2009 (H1N1) ^b	CC ₅₀ (μM) ^c MDCK cells	CC ₅₀ (μM) ^c A549 cells	T _{1/2} (min) ^d	CL _{int(liver)} (mL/min/kg)
 11	90.3 ± 3.4	11.2 ± 1.3	0.3 ± 0.1	100	177.5 ± 16.2	1.0	5290.9
 14	82.2 ± 2.3	N.T.	0.1 ± 0.03	>200	>300	31.5	174.1
 15	86.1 ± 1.9	N.T.	0.1 ± 0.04	>200	>200	13.4	410.4
 10a	85.4 ± 2.2	19.3 ± 2.5	0.2 ± 0.01	125.3 ± 8.2	130.3 ± 15.0	12.8	430.3
 10b	47.9 ± 1.0	2.3 ± 0.6	0.8 ± 0.05	>300	>300	>145	<38.0
 10c	57.6 ± 1.5	6.1 ± 0.5	1.7 ± 0.5	>300	>300	97.2	56.5
 10d	5.3 ± 2.9	N.T.	>30	>300	>300	N.T.	N.T.
 10e	44.8 ± 0.8	N.T.	3.1 ± 0.9	>300	>300	>145	<38.0
 10f	67.3 ± 3.2	10.2 ± 0.6	0.7 ± 0.1	>300	346.5 ± 19.2	N.T.	N.T.
 10g	33.8 ± 0.9	6.6 ± 1.6	2.6 ± 0.7	>300	>300	>145	<38.0
 8a	90.3 ± 0.6	N.T.	0.5 ± 0.1	102.3 ± 6.1	95.8 ± 3.6	N.T.	N.T.
 8b	87.2 ± 0.4	N.T.	0.6 ± 0.1	>300	>300	18.1	302.8
 8c	85.7 ± 1.6	8.4 ± 1.8	0.8 ± 0.1	9.0 ± 0.8	16.4 ± 2.7	N.T.	N.T.
 8d	84.3 ± 2.1	0.7 ± 0.5	0.3 ± 0.1	146.6 ± 62.8	>300	7.0	781.3
 8e	90.0 ± 1.7	N.T.	1.0 ± 0.1	7.5 ± 0.7	8.1 ± 0.7	N.T.	N.T.
 8f	89.9 ± 1.0	N.T.	0.5 ± 0.1	92.2 ± 4.7	189.5 ± 9.9	7.6	718.3

^aPercentage channel blockage is presented as the mean ± standard deviation of three independent experiments. ^bAntiviral assay was performed in plaque assay. The EC₅₀ values are the mean ± standard deviation of two independent experiments. ^cCytotoxicity was measured using the neutral red method with a 48 h incubation time.²⁵ The CC₅₀ values are the mean ± standard deviation of three independent experiments. ^dT_{1/2} was determined in mouse liver microsomes. N.T. = not tested.

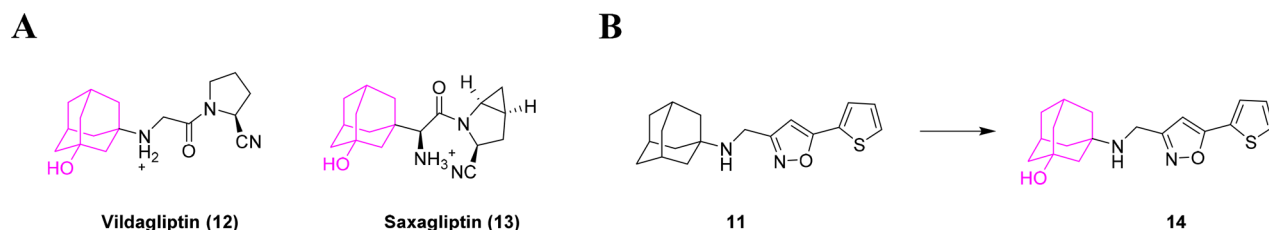


Figure 2. Hypothesis-driven optimization of the microsomal stability of AM2-S31N inhibitors. (A) Two FDA-approved oral drugs that contain the hydroxyl adamantane. (B) Strategy to increase the microsomal stability of AM2-S31N inhibitor 11.

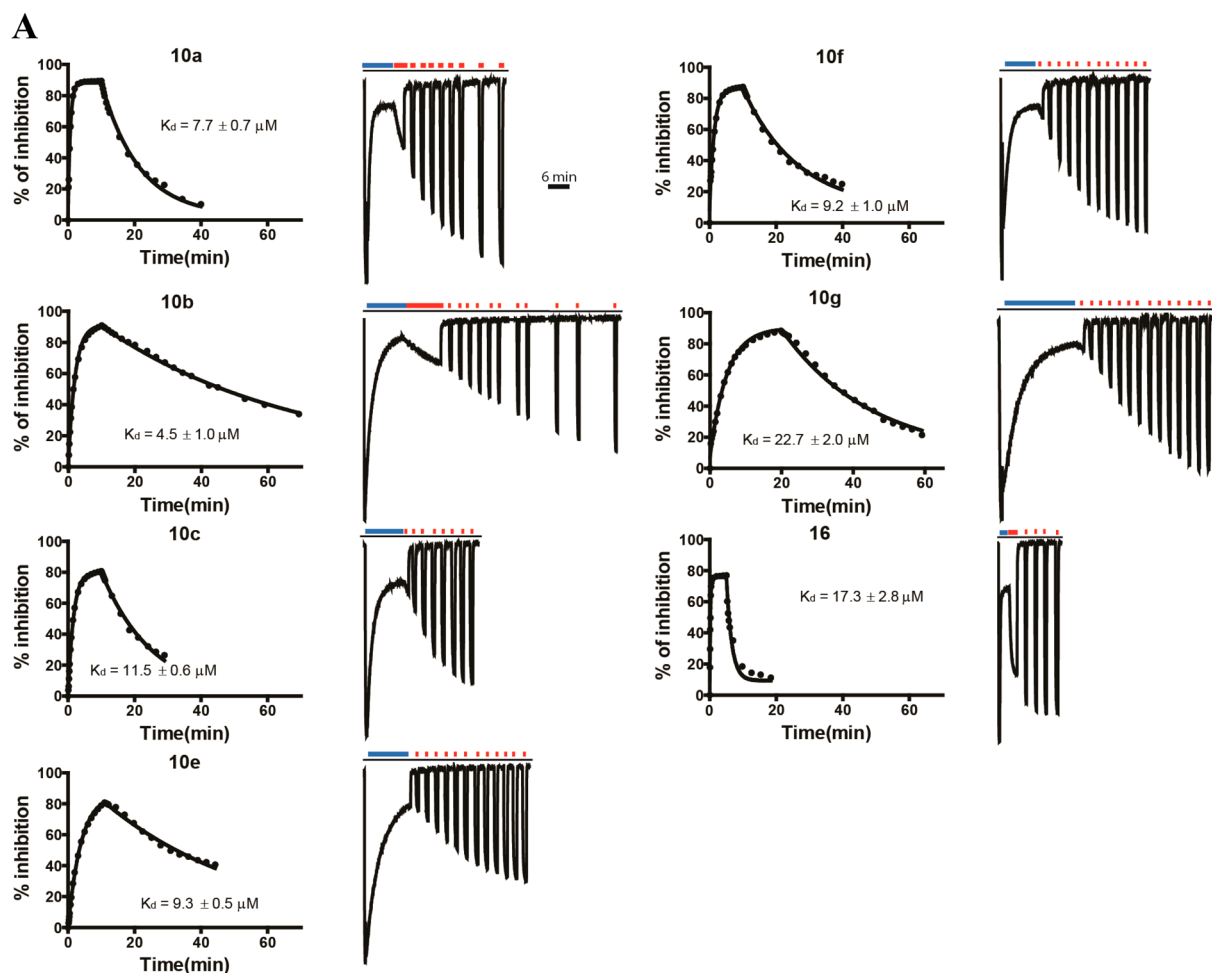
hydrogen bonds with the N31 side chain amide, and the adamantane cage fits in the cavity created by the G34 from AM2-S31N.

As a first step to optimize the *in vitro* PK properties of the AM2-S31N inhibitors, we profiled the mouse liver microsomal stability of compound 11, which is one of the most potent AM2-S31N inhibitors we have discovered so far (Table 1).¹⁹ It was found that compound 11 had an ultrashort half-life of 1.0 min in mouse liver microsomes, which excluded it from being tested in *in vivo* mouse studies. Inspection of the chemical structure of compound 11 revealed that there might be three possible metabolic soft spots: the adamantane, the isoxazole, and the thiophene.²⁰ Amantadine was shown to be metabolized to hydroxyl adamantane *in vivo*,²¹ the isoxazole ring can be cleaved at the N–O bond,²² and the thiophene ring is known to be easily oxidized.²³ To increase the microsomal stability of compound 11, we first searched the FDA-approved drug database for orally bioavailable adamantane-containing drugs, hoping to gain insights how to improve the microsomal stability of adamantane. The search revealed two compounds, vildagliptin (12) and saxagliptin (13) (Figure 2A), both of which are dipeptidyl peptidase-4 (DPP-4) inhibitors and are used as antidiabetic drugs. Vildagliptin (12) and saxagliptin (13) each contain hydroxyl adamantane instead of adamantane. The biological half-life $T_{1/2}$ of vildagliptin (12) and saxagliptin (13) were 2–3 and 2.5 h, respectively, following a single oral dose in healthy volunteers.²⁴ The presence of hydroxyl adamantane instead of adamantane in vildagliptin (12) and saxagliptin (13) might confer to their high microsomal stability and oral bioavailability. We therefore applied the same strategy in our PK optimization and converted compound 11 to the hydroxyl adamantane-containing compound 14 (Figure 2B). Compound 14 had similar channel blockage and antiviral efficacy as compound 11 (Table 1) and had an improved selectivity index over compound 11. Gratifyingly, the half-life of compound 14 in mouse microsomes was increased to 31.5 min. This result suggests that hydroxyl adamantane is indeed more metabolically stable than adamantane. Following the same rationale, we tested the mouse microsomal stability of another hydroxyl adamantane-containing AM2-S31N inhibitor, compound 15. The mouse microsomal half-life of compound 15 was 13.4 min, which was a significant improvement compared to compound 11 but still requires further optimization. Next, to remove another possible metabolic labile spot, the thiophene²³ in compounds 11, 14, and 15, we tested the microsomal stability of compound 10a, which contains a cyclopropyl substitution instead of thiophene. The mouse microsomal half-life of compound 10a was 12.8 min, which was a significant improvement compared to compound 11 ($T_{1/2}$ = 1.0 min). Substituting adamantane in 10a with hydroxyl adamantane gave compound 10b, which had a half-life of more than 145 min. Encouraged by this result, we then synthesized a few other

cyclopropyl-containing analogues 10c, 10d, 10e, 10f, and 10g. Compound 10d did not block the AM2-S31N channel (5.3% channel blockage at 100 μ M) and therefore had no antiviral activity. All other compounds (10c, 10e, 10f, and 10g) had potent antiviral activity (EC_{50} < 3.1 μ M) and a high selectivity index. Compounds 10c, 10e, and 10g were also stable in mouse microsomes with $T_{1/2}$ of 97.2, >145, and >145 min, respectively. Despite the potent antiviral activity of compounds 10b, 10c, 10e, 10f, and 10g, they had a moderate to weak channel blockage against the AM2-S31N channel (33.8–67.3% at 100 μ M). It is noteworthy that the value of percentage channel blockage reported herein was the value at the 2 min time point after applying 100 μ M of compound to the oocyte bathing medium. Therefore, this value may or may not represent the true binding potency of the compound because this experiment is under kinetic control. The apparent discrepancy between these compounds' weak to moderate percentage channel blockage at the 2 min time point and their potent antiviral activity suggest that they might be slow-binding inhibitors. To confirm this hypothesis, we performed detailed kinetic studies of these AM2-S31N inhibitors (10b, 10c, 10e, 10f, and 10g), and the results are shown in the next section.

In parallel, guided by the solution NMR structure of AM2-S31N in complex with compound 11 (PDB 2LY0) (Figure 1), we also designed and synthesized isoxazole adamantane analogues with cyclobutyl (8a, 8b), cyclopentyl (8c, 8d), and cyclohexyl (8e, 8f) substitutions. Substituting cyclopropyl with cyclobutyl, cyclopentyl, and cyclohexyl should be accommodated as this substitution forms hydrophobic interaction with the V27 side chain methyls (Figure 1). As expected, all compounds were found to have potent channel blockage against the AM2-S31N channel (>84% at 100 μ M) and potent antiviral activity against the AM2-S31N-containing A/California/07/2009 (H1N1) virus (EC_{50} \leq 1 μ M). However, replacing cyclopropyl in compound 10b with cyclobutyl (8b), cyclopentyl (8d), and cyclohexyl (8f) led to a gradual decrease of the mouse microsomal stability (Table 1). These results suggest cyclopropyl substitution is more metabolically stable than the corresponding cyclobutyl, cyclopentyl, and cyclohexyl substitutions.

Binding Kinetic Studies Of AM2-S31N Inhibitors. In our previous studies, we plotted the AM2-S31N inhibitors' percentage channel blockage at the 2 min time point with their antiviral activity in a plaque assay.¹⁵ It was found that compounds with a higher percentage of channel blockage normally have more potent antiviral efficacy. However, in this study, we found a few exceptions such as compounds 10b, 10c, 10e, 10f, and 10g, which all had moderate to weak channel blockage ranging from 33.8% to 67.3% at the 2 min time points when tested at 100 μ M drug concentration. According to the previous correlation, the predicted antiviral EC_{50} values of these compounds should have been greater than 8 μ M.¹⁵ However,



B

$$K_{ob} = [\text{compound}] * K_{on} + K_{off}$$

$$K_d = \frac{K_{off}}{K_{on}}$$

$$\text{Association} = B_{max} * \frac{[\text{compound}]}{[\text{compound}] + K_d} * (1 - \exp(-1 * K_{ob} * t))$$

$$Y@Time0 = B_{max} * \frac{[\text{compound}]}{[\text{compound}] + K_d} * (1 - \exp(-1 * K_{ob} * Time0))$$

$$\text{Dissociation} = Y@Time0 * \exp(-1 * K_{off} * (t - Time0))$$

$$Y = \text{IF}(X < \text{Time}0, \text{Association}, \text{Dissociation}) + \text{NS}$$

Y is the percent of inhibition at time *t*, *NS* is non-specific inhibition.

Figure 3. Kinetic studies of AM2-S31N inhibitors. (A) Binding and washing curves were recorded for two oocytes. One of the representative recording traces is shown. During the washing period, in order to prevent prolonged acidification of oocytes, a pH 5.5 pulse, instead of continuous application of pH 5.5 barth solution, was applied. The red bar shows when pH 5.5 pulse was applied, and the blue bar shows when 100 μM of compound was applied at pH 5.5. Nonlabeled areas shows when pH 8.5 solution was applied. (B) The association and dissociation equations used to fit the curves in A.

all of them had potent antiviral activity with EC_{50} values less than 3.1 μM . One possible explanation is that these compounds might be slow-binding inhibitors and equilibrium might not be achieved at the 2 min time point; therefore, the reported percentage channel blockage at the 2 min time point actually underestimates the true potency of these compounds. To validate this hypothesis, we chose compounds 10b, 10c, 10e, 10f, and 10g for detailed kinetic studies. Two additional

compounds 10a and 16 were included as controls for comparisons.

The K_d values of compounds 10a, 10b, 10c, 10e, 10f, 10g, and 16 were obtained by fitting the inhibition and washing curves (Figure 3A) with the association and dissociation equations (Figure 3B). All compounds were tested at 100 μM . The best-fit results are shown in Table 2. As shown in Figure 3A and Table 2, despite the moderate to low channel blockage at the 2 min time point for compounds 10b, 10c, 10e, and 10f

Table 2. Fitting Results from Kinetic Studies of AM2-S31N Inhibitors^a

Compounds	10a	10b	10c	10e	10f	10g	16
% AM2-S31N channel blockage at two-minute time point at 100 μ M	85.4 \pm 2.2	47.9 \pm 1.0	57.6 \pm 1.5	44.8 \pm 0.8	67.3 \pm 3.2	33.8 \pm 0.9	81.4 \pm 0.8
Antiviral EC ₅₀ (μ M)	0.2 \pm 0.01	0.8 \pm 0.05	1.7 \pm 0.5	3.1 \pm 0.9	0.7 \pm 0.1	2.6 \pm 0.7	6.8 \pm 0.7
cLogP ^b	3.406	2.561	2.353	1.847	3.509	2.521	5.024
Time0 (min)	10	10	10	11	10	20	5
B _{max} (max inhibition at equilibrium)	91.2 \pm 1.0	92.3 \pm 0.7	90.7 \pm 0.8	94.8 \pm 1.0	85.1 \pm 1.5	100	76.5 \pm 3.4
K _{on} (M ⁻¹ min ⁻¹)	13651 \pm 517	4754 \pm 121	5578 \pm 184	2378 \pm 83	6567 \pm 442	1745 \pm 102	41484 \pm 5439
K _{off} (min ⁻¹)	0.088 \pm 0.003	0.017 \pm 0.0003	0.064 \pm 0.002	0.022 \pm 0.0005	0.061 \pm 0.003	0.040 \pm 0.001	0.621 \pm 0.079
K _d (μ M)	7.7 \pm 0.7	4.5 \pm 1.0	11.5 \pm 0.6	9.3 \pm 0.5	9.2 \pm 1.0	22.7 \pm 2.0	17.3 \pm 2.8
Binding kinetics	Fast on, slow off	Slow on, slow off					Fast on, Fast off

^aThe best fit values for the inhibition by compounds **10a**, **10b**, **10c**, **10e**, **10f**, **10g**, and **16**. Results were obtained in Prism 5.0 using the equations shown in Figure 3B. The compound concentration was 100 μ M. The results are the mean \pm standard deviation of two independent experiments.

^bcLogP was calculated using the QikProp in Schrödinger Glide.

(44.8–67.3%), they had comparable K_d values (4.5–11.5 μ M) as the potent channel blocker compound **10a** (7.7 μ M). Consistent with our hypothesis, compounds **10b**, **10c**, **10e**, and **10f** are indeed slow-binding inhibitors as shown by their slow K_{on} ($<1 \times 10^4$ M⁻¹ min⁻¹) and slow K_{off} (<0.1 min⁻¹) values. Slow K_{off} is defined as the value being 10-fold lower than the fast K_{off} value. In contrast, compound **10a** has fast K_{on} ($>1 \times 10^4$ M⁻¹ min⁻¹) and slow K_{off} (<0.1 min⁻¹) values. Compound **10g** has the lowest K_{on} of 1745 \pm 102 M⁻¹min⁻¹ and the highest K_d of 22.7 \pm 2.0 μ M, yet it had potent antiviral activity with an EC₅₀ of 2.6 \pm 0.7 μ M. In contrast, compound **16** has both fast K_{on} ($>1 \times 10^4$ M⁻¹ min⁻¹) and fast K_{off} (>0.1 min⁻¹), with a K_d of 17.3 \pm 2.8 μ M.

In summary, on the basis of channel binding kinetics, AM2-S31N inhibitors can be grouped into three categories: (1) Compounds with fast K_{on} and slow K_{off} such as compound **10a**. This group of compounds normally has potent antiviral activity. In this case, the percentage channel blockage at the 2 min time point is an accurate predictor for the antiviral activity. (2) Compounds with slow K_{on} and slow K_{off} such as the newly discovered slow-binding inhibitors **10b**, **10c**, **10e**, **10f**, and **10g**. Compounds in this category may or may not have potent antiviral activity, which depends on their K_d values. Because of their slow K_{on} values, the percentage channel blockage at the 2 min time point cannot accurately predict the antiviral potency. (3) Compounds with fast K_{on} and fast K_{off} such as compound **16**. Similar to the slow-binding inhibitors, the antiviral potency of compounds in this category depends on their K_d values not their percentage inhibition at the 2 min time point.

It is noteworthy that although K_d values are more accurate predictors for the compounds' antiviral activity, in practice, it is not feasible to measure the K_d value for every compound. The reason for this is that K_d measurements require bathing AM2-S31N-expressing oocytes at pH 5.5 for an extended period of

time (>30 min), which often results in cell death and membrane leakage. On average, we could only obtain one quality binding and washing curve out of five measurements from different oocytes. Therefore, instead of simply filtering compounds based on their percentage channel blockage at the 2 min time point in the primary electrophysiological assays, all compounds should be tested in secondary antiviral plaque assays in parallel. In this way, potent compounds that show slow-binding kinetics in inhibiting AM2-S31N proton channel will not be mistakenly filtered.

Antiviral Activity of Compound 10b against Drug-Resistant Influenza A Viruses. The antiviral activity of compound **10b** was further tested against five additional human influenza A viruses, among which A/Denmark/528/2009 (H1N1), A/Washington/29/2009 (H1N1), A/Texas/04/2009 (H1N1), and A/North Carolina/29/2009 (H1N1) are resistant to both amantadine and oseltamivir carboxylate, while A/Switzerland/9715293/2013 (H3N2) is resistant to amantadine but sensitive to oseltamivir. These five strains, together with A/California/07/2009 (H1N1), all contain the AM2-S31N mutant. It was found that compound **10b** inhibited all six strains with EC₅₀ values less than 1 μ M (Figure 4). In addition, compound **10b** also showed potent inhibition against the AM2-S31N-containing A/WSN/33 (H1N1) virus with an EC₅₀ value of 0.5 \pm 0.2 μ M. The cytotoxicity CC₅₀ values of compound **10b** were greater than 300 μ M for both MDCK and A549 cells, which corresponds to a selectivity index of greater than 375. Overall, AM2-S31N inhibitors such as **10b** were shown to have potent antiviral activity against AM2-S31N-containing influenza A viruses with diverse genetic backgrounds.

In Vitro PK Profiling of Compound 10b. Given compound **10b**'s potent antiviral activity, high selectivity index, and long half-life in mouse microsomes, we further profiled other in vitro PK properties of compound **10b**, which

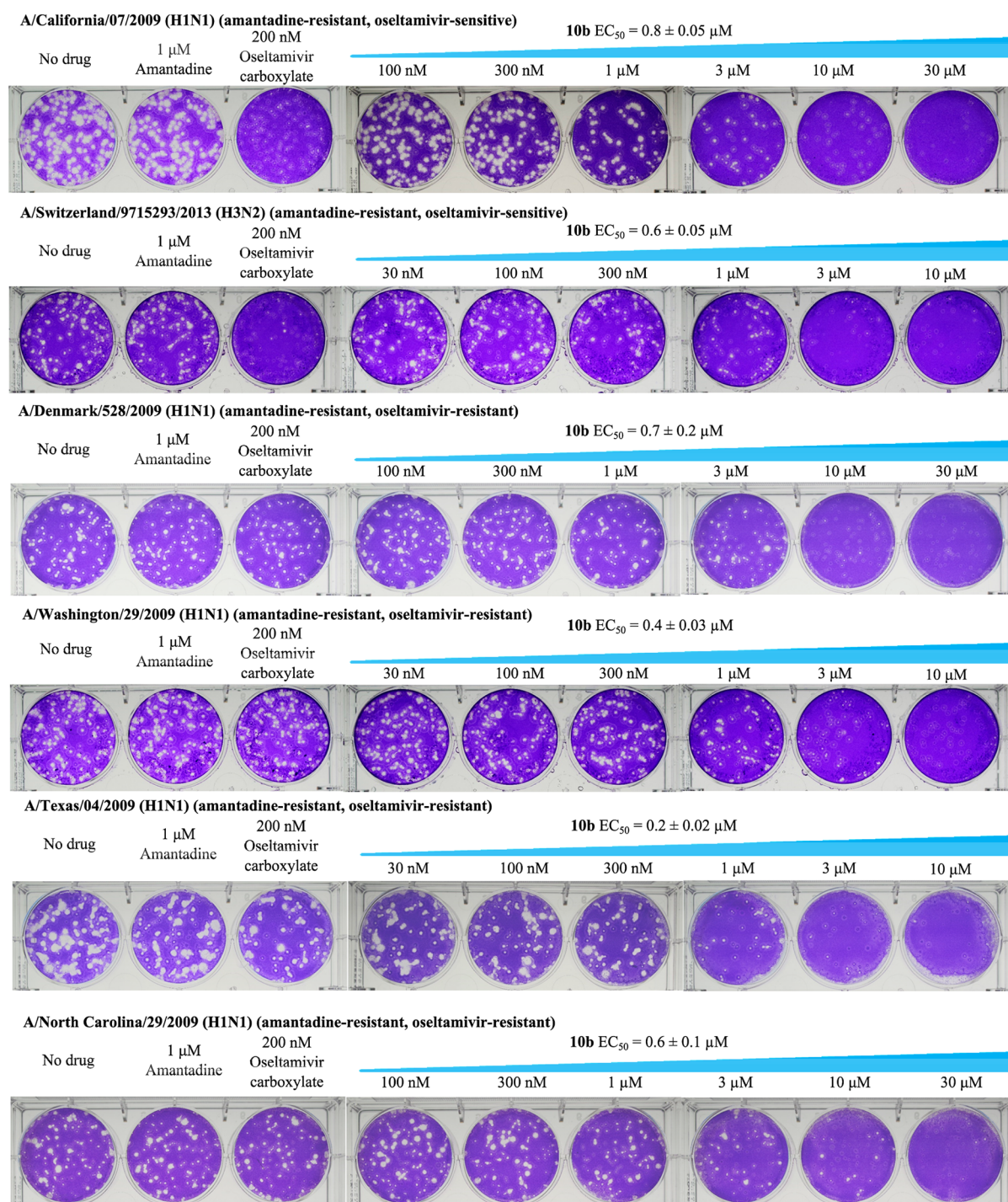
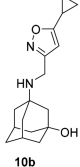


Figure 4. Plaque assays of compound **10b** in inhibiting human influenza A viruses. The EC_{50} values are the mean \pm standard deviation of two independent experiments. Representative plaque assay images from the one of the two independent experiments are shown.

include human liver microsome stability, cell permeability, and cytochrome P450 inhibition (Table 3). It was found that compound **10b** has high membrane permeability in Caco-2 cells, and it did not show inhibition against the five isoforms of CYP enzymes: 1A2, 2C9, 2C19, 2D6, and 3A4. Compound **10b** has a similar high stability in the human liver microsomes, with a half-life greater than 145 min. Compound **10b** also did not violate the Lipinski rule-of-five. In summary, the in vitro PK profiling predicts that compound **10b** will likely have high oral bioavailability.

Combination Therapy Potential of Compound **10b with Oseltamivir Carboxylate.** Combination therapy has been proven effective in decreasing the incidence of drug resistance as well as in lowering cytotoxicity.²⁶ As such, we are interested in exploring the combination therapy potential of AM2-S31N inhibitors such as **10b** with oseltamivir carboxylate. As AM2-S31N inhibitor **10b** targets a different viral replication stage than oseltamivir carboxylate, it is expected that a combination of compound **10b** with oseltamivir carboxylate will have a synergistic antiviral effect. To test this hypothesis, we applied the standard fractional inhibitory concentration

Table 3. In Vitro PK Properties of AM2-S31N Inhibitor 10b

Compound structure	Lipinski rule of five ^a	Permeability ($\times 10^{-6}$ cm/s) ^b	Mouse liver microsome stability $T_{1/2}$ (min)	Human liver microsome stability $T_{1/2}$ (min)	CYP inhibition ^c
	M.W. = 289.4 HBD = 3 HBA = 4 cLogP = 2.6	Caco-2 cells: A to B: 27.57 B to A: 28.33	>145	> 145	1A2: IC ₅₀ > 100 μ M 2C9: IC ₅₀ > 100 μ M 2C19: IC ₅₀ > 100 μ M 2D6: IC ₅₀ > 100 μ M 3A4: IC ₅₀ > 100 μ M

^aLipinski rule-of-five: MW < 500, HBD < 5, HBA < 10, clogP < 5; values were calculated using the QikProp in Schrödinger Glide. ^bBidirectional permeability in Caco-2 cells was assessed over a 120 min incubation at 37 °C and 5% CO₂ with saturated humidity; ^cCYP inhibition was tested at 10 μ M, and IC₅₀ was derived from the standard curve.

Table 4. Combination Therapy of 10b with Oseltamivir Carboxylate

combination ratio (EC ₅₀)	EC ₅₀ in combination		EC ₅₀ alone		EC ₅₀ equivalent ^a		FICI ^b	
	10b:oseltamivir	10b (μ M)	oseltamivir (nM)	10b (μ M)	oseltamivir (nM)	10b		oseltamivir
10:1		0.13 \pm 0.014	0.06 \pm 0.007			0.394	0.005	0.40
5:1		0.14 \pm 0.031	0.11 \pm 0.016			0.424	0.009	0.43
1:1		0.092 \pm 0.014	0.42 \pm 0.027	0.33 \pm 0.01	12.0 \pm 2.5	0.279	0.035	0.31
1:5		0.078 \pm 0.021	1.91 \pm 0.18			0.236	0.159	0.40
1:10		0.039 \pm 0.0044	1.97 \pm 0.22			0.118	0.164	0.28

^aConcentration in EC₅₀ equivalent was the normalized concentration that was calculated by dividing the EC₅₀ of drug in combination with its EC₅₀ alone. ^bFICI was the sum of 10b and oseltamivir EC₅₀-equivalent concentrations used in each combination.

index (FICI) method to evaluate the combination therapy effect of compound 10b with oseltamivir carboxylate.^{27–30} A FICI value of lower or higher than 1 indicates synergy or antagonism, respectively. It was found that all five sets of combination gave FICI less than 0.5 (Table 4), suggesting strong synergism by combining 10b with oseltamivir carboxylate. Among the five sets of results, a combination of 0.039 μ M 10b with 1.97 nM oseltamivir (combination ratio 1:10) exerted the highest synergistic efficacy with a FICI value of 0.28.

Docking Model of Compound 10b in AM2-S31N. To gain insight into how compound 10b binds to the AM2-S31N channel, we performed molecular modeling using the Schrödinger Glide standard precision docking. The solution NMR structure of AM2-S31N (PDB 2LY0) was used as the protein template. It was found that compound 10b can bind to the AM2-S31N channel in two different conformations (Figure 5A,B). In one conformation (Figure 5A), the isoxazole nitrogen from 10b forms a hydrogen bond with the N31 side chain amide NH₂ from one of the monomers, while the ammonium from 10b forms another hydrogen bond with the N31 side chain amide carbonyl from the opposite monomer. In the another binding confirmation (Figure 5B), the isoxazole nitrogen and ammonium from 10b form a bidentate hydrogen bond with the N31 side chain amide from one monomer. In both conformations (Figure 5A,B), the cyclopropyl substitution from 10b form hydrophobic interactions with the V27 side chain methyls, and the hydroxyl substitution on adamantane forms a hydrogen bond with the A30 backbone amide carbonyl.

CONCLUSIONS

Although novel drugs are urgently needed to address the unmet medical needs, drug discovery is unfortunately a lengthy and expensive venture.³¹ In the case of AM2-S31N drug discovery, no progress was made for decades until the report of the first-generation AM2-S31N inhibitors in 2013.^{19,32} Thereafter, lead optimization led to the development of more potent and

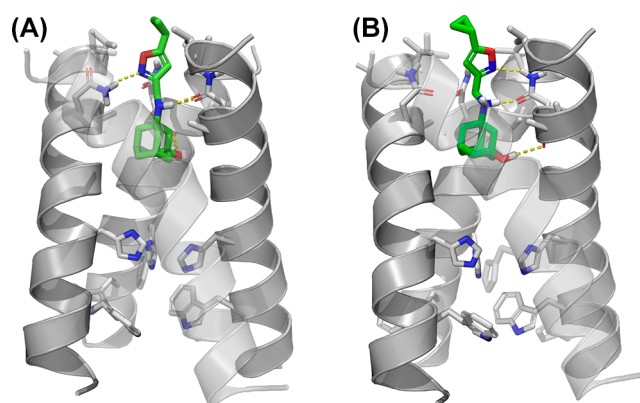


Figure 5. Docking models of compound 10b in the transmembrane domain of AM2-S31N (PDB 2LY0).¹⁹ The transparency of the front helix was set as 0.5 for clarity. Docking was performed using Schrödinger Glide standard precision.

selective AM2-S31N channel blockers that inhibit multiple strains of human influenza A viruses, including viruses that are resistant to amantadine, oseltamivir, or both. However, the first generation of AM2-S31N inhibitors such as compound 11 was found to have low stability in mouse microsomes, precluding them from further development. Guided by a hypothesis-driven approach, we were able to significantly improve the microsomal stability of AM2-S31N inhibitors. The lead compound 10b had a $T_{1/2}$ of more than 145 min in both mouse and human liver microsomes, and it was also highly permeable in Caco-2 cells and did not inhibit five isoforms of CYP. Interestingly, albeit the moderate percentage channel blockage ($47.9 \pm 1.0\%$) of compound 10b was at the 2 min time point when tested at 100 μ M, 10b had similar antiviral activity as compound 10a, which showed $85.4 \pm 2.2\%$ channel blockage at the 2 min time point when tested at 100 μ M. The potent antiviral activity of compound 10b was unexpected: according to previous

correlation study results, the predicted antiviral EC₅₀ value of compound **10b** would be more than 10 μM. However, in reality, compound **10b** inhibits multiple AM2-S31N-containing influenza A viruses with EC₅₀ values ranging from 0.2 to 0.8 μM (Figure 4). The apparent discrepancy led us to examine the binding kinetics of these AM2-S31N inhibitors. By fitting the binding and washing curves with the association and dissociation equations, we calculated the K_{on} , K_{off} , and K_d values of compounds **10a** and **10b**, along with a few other compounds (**10c**, **10e**, **10f**, **10g**, and **16**). The results showed that the newly discovered compounds **10b**, **10c**, **10e**, **10f**, and **10g** are slow-binding inhibitors and the binding equilibrium was not achieved at the 2 min time point when tested at 100 μM. Therefore, the reported percentage inhibition at the 2 min time point underestimates the true potency of these compounds (**10b**, **10c**, **10e**, **10f**, and **10g**). As such, although compound **10b** had significantly less percentage channel blockage than **10a** at the 2 min time point (47.9% versus 85.4%), they had similar K_d values (4.5 versus 7.7 μM). These results suggest that the K_d value is a more accurate predictor of the compound's antiviral activity rather than the percentage channel blockage at the 2 min time point.

Overall, the results presented herein may have important implications for other ion channel drug discovery program. As the electrophysiological assay is time-consuming, it is generally used as a primary assay to test compounds at a single drug concentration. However, as this process is under kinetic control, slow-binding inhibitors might be missed from this primary screening. To ensure slow-binding inhibitors are not being mistakenly filtered, functional assays should be performed in parallel.

In summary, this study led to the development of a promising lead compound (**10b**) with potent antiviral activity, high selectivity index, and favorable in vitro PK properties, and combination therapy of **10b** with oseltamivir carboxylate also showed strong synergism.

EXPERIMENTAL SECTION

Chemistry. Chemicals were ordered from commercial sources and were used without further purification. Synthesis procedures for reactions described in Scheme 1 were shown below. All final compounds were purified by flash column chromatography. ¹H and ¹³C NMR spectra were recorded on a Bruker-400 NMR spectrometer. Chemical shifts are reported in parts per million referenced with respect to residual solvent (CD₃OD) 3.31 ppm, (DMSO-*d*₆) 2.50 ppm, and (CDCl₃) 7.24 ppm or from internal standard tetramethylsilane (TMS) 0.00 ppm. The following abbreviations were used in reporting spectra: s, singlet; d, doublet; t, triplet; q, quartet; m, multiplet; dd, doublet of doublets; ddd, doublet of doublet of doublets. All reactions were carried out under N₂ atmosphere unless otherwise stated. HPLC-grade solvents were used for all reactions. Flash column chromatography was performed using silica gel (230–400 mesh, Merck). Low-resolution mass spectra were obtained using an ESI technique on a 3200 Q Trap LC/MS/MS system (Applied Biosystems). The purity was assessed by using a Shimadzu LC-MS with a Waters XTerra MS C-18 column (part no. 186000538), 50 mm × 2.1 mm, at a flow rate of 0.3 mL/min; λ = 250 and 220 nm; mobile phase A, 0.1% formic acid in H₂O, and mobile phase B', 0.1% formic in 60% 2-propanol, 30% CH₃CN, and 9.9% H₂O. All compounds submitted for testing in TEVC assay, plaque assay, cytotoxicity assay, and PK studies were confirmed to be >95.0% purity by LC-MS traces.

Synthesis Procedures. *Ethyl 5-Cyclopentyl-1,2-oxazole-3-carboxylate (4b)*. To a stirred solution of diethyl oxalate (1.46 g, 1.1 equiv) and 1-cyclopentylethanone (1.12g, 1 equiv) in toluene was added a solution of potassium *tert*-butoxide in THF (1.2 equiv)

dropwise. The resulting solution was stirred at room temperature overnight. The reaction was quenched with 1 N HCl and extracted with ethyl acetate (3×). The combined organic layers were dried over MgSO₄, filtered, and concentrated under reduced pressure. The crude product was dissolved in methanol, and hydroxylamine hydrochloride (1.04g, 1.5 equiv) was added. The solution was heated to 50 °C for 6 h. The solvent was removed under reduced pressure, and the resulting isoxazole ester was purified by flash column chromatography (10–20% EtOAc/hexane) to give the final product as a white solid. Yield: 56%. ¹H NMR (400 MHz, CDCl₃) δ 6.37 (s, 1H), 4.40 (q, *J* = 7.2 Hz, 2H), 3.26–3.18 (m, 1H), 2.11–2.05 (m, 2H), 1.79–1.62 (m, 6H), 1.37 (t, *J* = 7.2 Hz, 3H). C₁₁H₁₅NO₃ EI-MS: *m/z* (M + H⁺): 210.2 (calculated), 210.0 (found).

3-(Bromomethyl)-5-cyclopentyl-1,2-oxazole (6b). The ester **4b** (0.21g, 1 equiv) was dissolved in methanol and cooled down to 0 °C. NaBH₄ (0.15g, 4 equiv) was added in small portions to the solution over 10 min. The mixture was warmed to room temperature and stirred for 4 h. The reaction was quenched by adding diluted HCl, and the organic solvent was removed under reduced pressure. The resulting aqueous layer was extracted with ethyl acetate (3×), and the organic layers were combined and dried over MgSO₄, and the solvent was removed under reduced pressure. This hydroxyl intermediate **5b** was used for the next step without further purification. Hydroxyl intermediate (0.17 g, 1 equiv) was dissolved in DCM, and the resulting solution was cooled down to 0 °C. CBr₄ (0.50g, 1.5 equiv) and PPh₃ (0.39 g, 1.5 equiv) were added sequentially. The solution was stirred at 0 °C for 20 min and gradually warmed up to room temperature. The solvent was removed under reduced pressure, and the residue was purified by flash column chromatography (20% hexane/DCM) to give the desired intermediate **6b**. Yield: 62%. ¹H NMR (400 MHz, CDCl₃) δ 6.06 (s, 1H), 4.39 (s, 2H), 3.24–3.15 (m, 1H), 2.14–2.05 (m, 2H), 1.83–1.65 (m, 6H). C₉H₁₂BrNO EI-MS: *m/z* (M + H⁺): 231.1 (calculated), 231.0 (found).

3-(Bromomethyl)-5-cyclobutyl-1,2-oxazole (6a). The synthesis and characterization of bromide **6a** was reported.¹⁸

3-(Bromomethyl)-5-cyclohexyl-1,2-oxazole (6c). The synthesis and characterization of bromide **6c** was reported.¹⁸

General Procedure of Alkylations. The bromide (1 equiv) and amantadine or 1-amino-3-hydroxyadamantane or 5-aminoadamantan-2-one (1.5 equiv) were dissolved in 2-propanol; CsI (0.1 equiv) and triethyl amine (2 equiv) were then added. The reaction mixture was heated to reflux overnight. The solvent was removed under reduced pressure, and the resulting residue was extracted with ethyl acetate and water. The organic layer was separated, dried over anhydrous MgSO₄, filtered, and concentrated under reduced pressure. The mixture was then purified by silica gel flash column chromatography (5–10% CH₃OH/CH₂Cl₂) to give the final product.

N-[(5-Cyclobutyl-1,2-oxazol-3-yl)methyl]adamantan-1-amine (8a). Compound **8a** was synthesized according to the above-described alkylation procedure starting with bromide **6a**. The characterization of compound **8a** was reported before.¹⁸

3-[[5-(5-Cyclobutyl-1,2-oxazol-3-yl)methyl]amino]adamantan-1-ol (8b). Compound **8b** was synthesized according to the above-described alkylation procedure starting with bromide **6a**. Yield: 78%. ¹H NMR (400 MHz, CDCl₃): δ 6.03 (s, 1H), 3.83 (s, 2H), 3.63–3.55 (m, 1H), 2.41–2.31 (m, 2H), 2.31–2.21 (m, 4H), 2.10–1.90 (m, 4H), 1.72–1.64 (m, 6H), 1.64–1.59 (m, 4H), 1.55–1.50 (m, 2H). ¹³C NMR (100 MHz, CDCl₃): δ 176.51, 163.24, 99.27, 69.64, 54.51, 50.00, 44.34, 41.07, 37.01, 35.09, 32.07, 30.73, 28.00, 18.74. C₁₈H₂₆N₂O₂ EI-MS: *m/z* (M + H⁺): 303.4 (calculated), 303.0 (found).

N-[(5-Cyclopentyl-1,2-oxazol-3-yl)methyl]adamantan-1-amine (8c). Compound **8c** was synthesized according to the above-described alkylation procedure starting with bromide **6b**. Yield: 75%. ¹H NMR (400 MHz, CDCl₃ + CD₃OD): δ 6.85 (s, 1H), 4.22–4.15 (m, 2H), 3.20–3.08 (m, 1H), 2.17–2.10 (m, 3H), 2.08–2.02 (m, 6H), 2.02–1.95 (m, 2H), 1.75–1.61 (m, 12H). ¹³C NMR (100 MHz, CDCl₃): δ 178.91, 157.08, 100.94, 59.01, 38.73, 37.48, 35.85, 35.38, 31.84, 29.14, 25.24. C₁₉N₂₈N₂O EI-MS: *m/z* (M + H⁺): 301.4 (calculated), 301.0 (found).

3-[[5-(5-Cyclopentyl-1,2-oxazol-3-yl)methyl]amino]adamantan-1-ol (**8d**). Compound **8d** was synthesized according to the above-described alkylation procedure starting with bromide **6b**. Yield: 82%. ¹H NMR (400 MHz, CDCl₃ + CD₃OD): δ 6.71 (s, 1H), 4.20–4.11 (m, 2H), 3.23–3.12 (m, 1H), 2.40–2.32 (m, 2H), 2.14–1.99 (m, 4H), 1.98–1.85 (m, 4H), 1.81–1.61 (m, 10H), 1.59–1.50 (m, 2H). ¹³C NMR (100 MHz, CDCl₃): δ 180.05, 155.89, 100.68, 68.50, 60.21, 42.73, 37.44, 36.66, 34.17, 31.80, 30.19, 25.20. C₁₉H₂₈N₂O₂ EI-MS: *m/z* (M + H⁺): 317.4 (calculated), 317.0 (found).

N-[[5-(5-Cyclohexyl-1,2-oxazol-3-yl)methyl]amino]adamantan-1-amine (**8e**). Compound **8e** was synthesized according to the above-described alkylation procedure starting with bromide **6c**. The characterization of compound **8e** was reported before.¹⁸

3-[[5-(5-Cyclohexyl-1,2-oxazol-3-yl)methyl]amino]adamantan-1-ol (**8f**). Compound **8f** was synthesized according to the above-described alkylation procedure starting with bromide **6c**. Yield: 85%. ¹H NMR (400 MHz, CD₃Cl + CD₃OD): δ 6.57 (s, 1H), 4.19–4.02 (m, 2H), 2.80–2.63 (m, 1H), 2.43–2.24 (m, 2H), 2.06–1.79 (m, 8H), 1.79–1.58 (m, 7H), 1.59–1.45 (m, 2H), 1.45–1.16 (m, 5H). ¹³C NMR (100 MHz, CDCl₃+CD₃OD): δ 180.06, 155.59, 100.11, 68.79, 60.48, 42.68, 36.70, 36.31, 35.30, 34.10, 30.89, 30.11, 25.55, 25.47. C₂₀H₃₀N₂O₂ EI-MS: *m/z* (M + H⁺): 331.5 (calculated), 332.0 (found).

Compounds **10a–10g** were synthesized using the general alkylation procedure described above starting from commercial available bromides.

N-[[5-(5-Cyclopropyl-1,2-oxazol-3-yl)methyl]amino]adamantan-1-amine (**10a**). The characterization of **10a** was reported before.¹⁹

3-[[5-(5-Cyclopropyl-1,2-oxazol-3-yl)methyl]amino]adamantan-1-ol (**10b**). Yield: 72%. ¹H NMR (400 MHz, CDCl₃): δ 5.92 (s, 1H), 3.83 (s, 2H), 2.29–2.23 (m, 2H), 2.02–1.91 (m, 2H), 1.68–1.63 (m, 5H), 1.61–1.57 (m, 4H), 1.53–1.48 (m, 2H), 1.05–0.98 (m, 2H), 0.95–0.89 (m, 2H). ¹³C NMR (100 MHz, CDCl₃): δ 174.76, 164.18, 98.63, 70.25, 54.02, 50.16, 44.26, 41.31, 36.88, 35.41, 30.98, 8.29, 8.08. C₁₇H₂₄N₂O₂ EI-MS: *m/z* (M + H⁺): 289.4 (calculated), 289.0 (found).

5-[[5-(5-Cyclopropyl-1,2-oxazol-3-yl)methyl]amino]adamantan-2-one (**10c**). Yield: 80%. ¹H NMR (400 MHz, CDCl₃): δ 5.88 (s, 1H), 3.76 (s, 2H), 2.60–2.53 (m, 2H), 2.28–2.21 (m, 1H), 2.00–1.87 (m, 11H), 1.04–0.97 (m, 2H), 0.93–0.87 (m, 2H). ¹³C NMR (100 MHz, CDCl₃): δ 217.3, 175.03, 163.72, 98.46, 50.75, 46.64, 43.00, 41.69, 38.62, 37.42, 28.90, 8.67, 8.62. C₁₇N₂O₂ EI-MS: *m/z* (M + H⁺): 287.4 (calculated), 287.0 (found).

3-[[5-(5-Cyclopropyl-1,3,4-oxadiazol-2-yl)methyl]amino]adamantan-1-ol (**10d**). Yield: 71%. ¹H NMR (400 MHz, CDCl₃): δ 3.97 (s, 2H), 2.32–2.23 (m, 2H), 2.16–2.05 (m, 1H), 1.68–1.61 (m, 6H), 1.60–1.55 (m, 4H), 1.53–1.47 (m, 2H), 1.13–1.11 (m, 2H), 1.11–1.09 (m, 2H). ¹³C NMR (100 MHz, CDCl₃): δ 168.50, 164.95, 69.48, 53.78, 49.61, 43.95, 40.74, 35.99, 34.60, 30.55, 7.87, 5.70. C₁₆H₂₃N₃O₂ EI-MS: *m/z* (M + H⁺): 290.4 (calculated), 290.0 (found).

3-[[5-(5-Cyclopropyl-1,2,4-oxadiazol-3-yl)methyl]amino]adamantan-1-ol (**10e**). Yield: 84%. ¹H NMR (400 MHz, CDCl₃ + CD₃OD): δ 4.15 (s, 2H), 2.35–2.28 (m, 2H), 2.22–2.12 (m, 1H), 1.96–1.90 (m, 2H), 1.89–1.78 (m, 4H), 1.70–1.61 (m, 4H), 1.54–1.47 (m, 2H), 1.26–1.16 (m, 4H). ¹³C NMR (100 MHz, CDCl₃ + CD₃OD): δ 183.64, 162.35, 68.08, 60.75, 45.82, 42.45, 36.75, 35.34, 33.85, 30.28, 10.53, 7.18. C₁₆H₂₃N₃O₂ EI-MS: *m/z* (M + H⁺): 290.4 (calculated), 290.0 (found).

N-[[5-(5-Cyclopropyl-1,3,4-thiadiazol-2-yl)methyl]amino]adamantan-1-amine (**10f**). Yield: 78%. ¹H NMR (400 MHz, CDCl₃): δ 4.18 (s, 2H), 2.42–2.34 (m, 1H), 2.14–2.08 (m, 3H), 1.74–1.67 (m, 9H), 1.67–1.60 (m, 3H), 1.25–1.18 (m, 2H), 1.12–1.06 (m, 2H). ¹³C NMR (100 MHz, CDCl₃): δ 174.15, 42.42, 40.17, 36.45, 29.48, 11.65, 11.38. C₁₆H₂₃N₃S EI-MS: *m/z* (M + H⁺): 290.4 (calculated), 290.0 (found).

3-[[5-(5-Cyclopropyl-1,3,4-thiadiazol-2-yl)methyl]amino]adamantan-1-ol (**10g**). Yield: 78%. ¹H NMR (400 MHz, DMSO-*d*₆): δ 4.66 (s, 2H), 2.63–2.55 (m, 1H), 2.30–2.23 (m, 2H), 1.82–1.76 (m, 6H), 1.61–1.50 (m, 4H), 1.50–1.43 (m, 2H), 1.29–1.22 (m, 2H), 1.06–1.00 (m, 2H). ¹³C NMR (100 MHz, DMSO-*d*₆): δ 175.97,

67.82, 59.95, 54.82, 46.05, 43.87, 37.93, 36.93, 34.30, 30.13, 12.04, 11.42. C₁₆H₂₃N₃OS EI-MS: *m/z* (M + H⁺): 306.4 (calculated), 306.0 (found).

Characterization of compounds **11**, **14**, **15**, and **16** was reported before.^{16,18,19}

Two-Electrode Voltage Clamp (TEVC) Assay. The compounds were tested in a two-electrode voltage clamp assay using *Xenopus laevis* frog oocytes microinjected with RNA expressing either the AM2-WT or the AM2-S31N mutant of the AM2 protein, as previously reported.³³ The M2 sequences used for this study were identical to the A/California/07/2009 (H1N1) M2 sequence (AM2-S31N) and the corresponding AM2-N31S mutant (AM2-WT). The M2 sequences from A/WSN/33 (H1N1) and A/California/07/2009 (H1N1) differ only by one amino acid at the transmembrane region at position 28: in A/WSN/33 (H1N1) is valine and in A/California/07/2009 (H1N1) is isoleucine. The potency of the inhibitors was expressed as percentage inhibition of AM2 current observed after 2 min of incubation with 100 μM of compounds at pH 5.5. All measurements were repeated three times with different oocytes. For kinetic studies, during the binding period, the oocyte was fluxed with pH 5.5 buffer containing 100 μM of compound until binding equilibrium was achieved. During the washing period, in order to prevent prolonged acidification of oocytes, a pH 5.5 pulse, instead of continuous application of pH 5.5 bath solution, was applied until equilibrium was achieved.

Plaque Assay. The plaque assay was performed as previously reported^{29,30} except MDCK cells expressing ST6Gal I were used instead of regular MDCK cells.³⁴ Briefly, a confluent monolayer of ST6Gal I MDCK cells was incubated with ~100 pfu virus/well in DMEM with 0.5% BSA for 1 h at 4 °C then at 37 °C for 1 h. The inoculums were removed, and the cells were washed with phosphate buffered saline (PBS). The cells were then overlaid with DMEM containing 1.2% Avicel microcrystalline cellulose (FMC BioPolymer, Philadelphia, PA) and NAT (2.0 μg/mL). To examine the effect of the compounds on plaque formation, the overlay media was supplemented with compounds at testing concentrations. After 2 days of incubation at 37 °C with 5% of CO₂ in the cell culture incubator, the overlay was removed and the cell monolayers were fixed and stained with crystal violet dye solution (0.2% crystal violet, 20% methanol). Influenza A viruses A/Switzerland/9715293/2013 X-247 (H3N2), FR-1366, A/Washington/29/2009 (H1N1), FR-460, A/North Carolina/29/2009 (H1N1), FR-488, and A/California/07/2009 (H1N1), FR-201, were obtained through the Influenza Reagent Resource, Influenza Division, WHO Collaborating Center for Surveillance, Epidemiology and Control of Influenza, Centers for Disease Control and Prevention, Atlanta, GA, USA. Influenza virus A/Denmark/528/2009 (H1N1) was obtained from Dr. Elena Govorkova at St. Jude Children's Research Hospital. Influenza virus A/Texas/04/2009 (H1N1) was obtained from Dr. James Noah at the Southern Research Institute.

Cytotoxicity Assay. Evaluation of the cytotoxicity of compounds and the efficacy of compounds against influenza-induced cytopathic effect was carried out using the neutral red uptake assay.²⁵ Briefly, 80000 cells/mL of MDCK or A549 cells in DMEM medium supplemented with 10% FBS and 100 U/mL penicillin–streptomycin were dispensed into 96-well cell culture plates at 100 μL/well. Then 24 h later, the growth medium was removed and washed with 100 μL of PBS buffer, then for the cytotoxicity assay, 200 μL of fresh DMEM (no FBS) medium containing serial diluted compounds was added to each well. After incubating for 48 h at 37 °C with 5% CO₂ in a CO₂ incubator, the medium was removed, and then 100 μL of DMEM medium containing 40 μg/mL neutral red was added and the plate was incubated for 4 h at 37 °C. The amount of uptaken neutral red was determined at absorbance 540 nm using a Multiskan FC microplate photometer (Fisher Scientific). The CC₅₀ values were calculated from best-fit dose response curves with variable slope in GraphPad Prism version 5.

Combination Therapy of Compound 10b with Oseltamivir Carboxylate. The synergistic antiviral effect of compound **10b** and oseltamivir carboxylate was evaluated in cell cultures as described previously using CPE assay.^{29,30} Five combinations of compound **10b**

and oseltamivir carboxylate, at the fixed EC_{50} ratios of 10:1, 5:1, 1:1, 1:5, and 1:10, were included. In each combination, a stock solution with the designated EC_{50} ratio of compound **10b** and oseltamivir carboxylate was first made, then six 3-fold serial dilutions of the stock solution were made and tested to obtain the dose–response curve, based on which EC_{50} of individual **10b** or oseltamivir carboxylate was determined. Subsequently, fractional inhibitory concentration index (FICI) was calculated using the following formula: $FICI = ((EC_{50} \text{ of } \mathbf{10b} \text{ in combination}) / (EC_{50} \text{ of } \mathbf{10b} \text{ alone})) + ((EC_{50} \text{ of oseltamivir carboxylate in combination}) / (EC_{50} \text{ of oseltamivir carboxylate alone}))$. $FICI < 0.5$ was interpreted as a significant synergistic antiviral effect.

Microsome Stability. Test compounds were incubated at 37 °C with liver microsomes (mouse or human) (Xenotech) at 1 μ M drug concentration in the presence of a NADPH regenerating system at 0.5 mg/mL microsomal protein. Testosterone (3A4 substrate), propafenone (2D6), and diclofenac (2C9) were included as positive controls. Compounds were incubated with microsomes in the presence of a NADPH regenerating system (Sigma, catalogue no. N0505, lot SLBH3107V). Aliquots at 0, 5, 10, 20, 30, and 60 min post incubation were collected and immediately mixed with cold acetonitrile containing internal standard (IS). Compounds incubated with microsomes without NADPH regenerating system for 60 min were also included. All the samples were analyzed by LC/MS/MS; disappearance of test compound were assessed based on peak area ratios of analyte/IS. Following equations were applied to calculate the microsome clearance:

elimination rate constant (k) = $-\text{gradient}$;

$$\text{half life } (T_{1/2}) \text{ (min)} = \frac{0.693}{k}$$

$CL_{\text{int(mic)}} = 0.693/\text{half-life}/\text{mg microsome protein per mL}$. Liver wt: 40, 30, 32, 20, and 88 g/kg for rat, monkey, dog, human, and mouse. Using $CL_{\text{int(mic)}}$ to calculate the whole the liver clearance: mg microsomal protein/g liver weight, 45 mg/g for five species. $CL_{\text{int(liver)}} = CL_{\text{int(mic)}} \times \text{mg microsomal protein/g liver weight} \times \text{g liver weight/kg body weight}$.

Caco-2 Cell Permeability Assay. Caco-2 cells (ATCC) were cultured in MEM with 10% FBS. Cells at the passage number from 30 to 50 are seeded onto PET membranes of 96-well insert plates at 1×10^5 cells/cm² for 21–28 days to reach confluent cell monolayer. The integrity of the monolayer was verified by performing Lucifer yellow rejection assay. The quality of the monolayer were verified by measuring the unidirectional (A \rightarrow B) permeability of fenoterol (low permeability marker), propranolol (high permeability marker), and bidirectional permeability of digoxin (a P-glycoprotein substrate marker) in duplicate wells. Assay conditions for test compounds listed are as follows:

- Test concentration: 2 μ M (DMSO \leq 1%)
- Replicates: $n = 2$
- Directions: bidirectional transport including A \rightarrow B and B \rightarrow A
- Incubation time: single time point, 2 h
- Transport buffer: HBSS containing 10 mM HEPES, pH 7.4
- Incubation condition: 37 °C, 5% CO₂, 95% relative humidity

Testing compounds were diluted in transport buffer and acetonitrile (containing internal standard), and the resulting solution is designated as the T0 sample. At the end of incubation, sample solutions from both donor and receiver wells were immediately mixed with cold acetonitrile containing internal standard (IS). All samples, including T0 samples, donor samples, and receiver samples, were analyzed using LC/MS/MS. Concentrations of test compound were expressed as peak area ratio of analytes versus IS without a standard curve.

The apparent permeability coefficient P_{app} (cm/s) was calculated using the equation:

$$P_{\text{app}} = (dC_r/d_t) \times V_r / (A \times C_0)$$

Where dC_r/d_t is the cumulative concentration of compound in the receiver chamber as a function of time (μ M/s), V_r is the solution volume in the receiver chamber (0.075 mL on the apical side, 0.25 mL

on the basolateral side), A is the surface area for the transport, i.e., 0.0804 cm² for the area of the monolayer, and C_0 is the initial concentration in the donor chamber (μ M).

CYP Inhibition. Compound was incubated at 10 μ M with human liver microsomes with protein concentration at 0.253 mg/mL. α -Naphthoflavone, sulfaphenazole, (+)-*N*-3-benzylirvanol, quinidine, and ketoconazole were used as positive controls. The mixture of test compound or positive control were prewarmed with human liver microsomes at 37 °C for 10 min. Phenacetin, diclofenac, *S*-mephenytoin, dextromethorphan, and midazolam were mixed and were used as substrates of CYP1A2, 2C9, 2C19, 2D6, and 3A4, respectively. After addition of substrate mixture and cofactor NADPH, the solution was incubated for another 10 min. The samples were then quenched with stop solution containing internal standard. Next, the solution was centrifuged at 4000 rpm (Centrifuge, 5810R Eppendorf) at room temperature for 20 min. The supernatant was diluted with purified water (v/v 2:1), which was shaken at 1000 rpm (Titer plate shaker, Thermo) for 10 min before LC-MS/MS injection. The formation of the metabolites acetaminophen, 4'-hydroxy diclofenac, 4'-hydroxy mephenytoin, dextrorphan, and 1'-hydroxy midazolam were determined by LC-MS/MS and IC_{50} values were calculated. SigmaPlot (V.11) was used to plot the mean CYP activity (% VC) versus the test compound concentrations with nonlinear regression analysis. IC_{50} values were reported as " $>100 \mu$ M" when % inhibition at highest concentration (100 μ M) was less than 50%.

The IC_{50} values were extrapolated using the following equation:

$$IC_{50} = x(100 - \% \text{inhibition at } x) / \% \text{inhibition}$$

suppose Hill slope = 1, where x = concentration of test compounds.

■ ASSOCIATED CONTENT

📄 Supporting Information

The Supporting Information is available free of charge on the ACS Publications website at DOI: 10.1021/acs.jmedchem.7b01536.

Molecular formula strings (CSV)

Docking model for **10b** (Figure 5A) (PDB)

Docking model for **10b** (Figure 5B) (PDB)

■ AUTHOR INFORMATION

Corresponding Author

*Phone: 520-626-1366. Fax: 520-626-0749. E-mail: junwang@pharmacy.arizona.edu.

ORCID

Jun Wang: 0000-0002-4845-4621

Author Contributions

¹Yuanxiang Wang and Yanmei Hu contributed equally to this work

Notes

The authors declare no competing financial interest.

■ ACKNOWLEDGMENTS

This research is supported by startup funding from the University of Arizona and NIH grant AI119187 to J.W. R.M. was supported by the NIH training grant T32 GM008804. We thank Dr. David Bishop for proofreading and editing the manuscript.

■ ABBREVIATIONS USED

WT, wild type; DMEM, Dulbecco's Modified Eagle Medium; MDCK, Madin–Darby canine kidney; TEVC, two-electrode voltage clamps

REFERENCES

- (1) Webster, R. G.; Monto, A. S.; Braciale, T. J.; Lamb, R. A. *Textbook of Influenza*; John Wiley & Sons, Ltd: West Sussex, UK, 2013.
- (2) Zhang, W. Q.; Webster, R. G. Can we beat influenza? *Science* **2017**, *357*, 111–111.
- (3) Zhu, H.; Lam, T. T.; Smith, D. K.; Guan, Y. Emergence and development of H7N9 influenza viruses in China. *Curr. Opin. Virol.* **2016**, *16*, 106–113.
- (4) Lai, S.; Qin, Y.; Cowling, B. J.; Ren, X.; Wardrop, N. A.; Gilbert, M.; Tsang, T. K.; Wu, P.; Feng, L.; Jiang, H.; Peng, Z.; Zheng, J.; Liao, Q.; Li, S.; Horby, P. W.; Farrar, J. J.; Gao, G. F.; Tatem, A. J.; Yu, H. Global epidemiology of avian influenza A H5N1 virus infection in humans, 1997–2015: a systematic review of individual case data. *Lancet Infect. Dis.* **2016**, *16*, e108–118.
- (5) *People at High Risk of Developing Flu-Related Complications*; Centers for Disease Control and Prevention: Atlanta, GA, 2018; https://www.cdc.gov/flu/about/disease/high_risk.htm (accessed on November 20, 2017).
- (6) Shaw, M. L. The next wave of influenza drugs. *ACS Infect. Dis.* **2017**, *3*, 691–694.
- (7) Wang, J.; Li, F.; Ma, C. Recent progress in designing inhibitors that target the drug-resistant M2 proton channels from the influenza A viruses. *Biopolymers* **2015**, *104*, 291–309.
- (8) Loregian, A.; Mercorelli, B.; Nannetti, G.; Compagnin, C.; Palu, G. Antiviral strategies against influenza virus: towards new therapeutic approaches. *Cell. Mol. Life Sci.* **2014**, *71*, 3659–3683.
- (9) Wang, J.; Qiu, J. X.; Soto, C.; DeGrado, W. F. Structural and dynamic mechanisms for the function and inhibition of the M2 proton channel from influenza A virus. *Curr. Opin. Struct. Biol.* **2011**, *21*, 68–80.
- (10) Gubareva, L. V.; Besselaar, T. G.; Daniels, R. S.; Fry, A.; Gregory, V.; Huang, W.; Hurt, A. C.; Jorquera, P. A.; Lackenby, A.; Leang, S. K.; Lo, J.; Pereyaslov, D.; Rebelo-de-Andrade, H.; Siqueira, M. M.; Takashita, E.; Odagiri, T.; Wang, D.; Zhang, W.; Meijer, A. Global update on the susceptibility of human influenza viruses to neuraminidase inhibitors, 2015–2016. *Antiviral Res.* **2017**, *146*, 12–20.
- (11) Webster, R. G.; Govorkova, E. A. Continuing challenges in influenza. *Ann. N. Y. Acad. Sci.* **2014**, *1323*, 115–139.
- (12) Hurt, A. C. The epidemiology and spread of drug resistant human influenza viruses. *Curr. Opin. Virol.* **2014**, *8*, 22–29.
- (13) Matsuzaki, Y.; Mizuta, K.; Aoki, Y.; Suto, A.; Abiko, C.; Sanjoh, K.; Sugawara, K.; Takashita, E.; Itagaki, T.; Katsushima, Y.; Ujike, M.; Obuchi, M.; Odagiri, T.; Tashiro, M. A two-year survey of the oseltamivir-resistant influenza A(H1N1) virus in Yamagata, Japan and the clinical effectiveness of oseltamivir and zanamivir. *Virol. J.* **2010**, *7*, 53.
- (14) Dong, G.; Peng, C.; Luo, J.; Wang, C.; Han, L.; Wu, B.; Ji, G.; He, H. Adamantane-resistant influenza A viruses in the world (1902–2013): frequency and distribution of M2 gene mutations. *PLoS One* **2015**, *10*, e0119115.
- (15) Li, F.; Hu, Y.; Wang, Y.; Ma, C.; Wang, J. Expedient lead optimization of isoxazole-containing influenza A virus M2-S31N inhibitors using the Suzuki-Miyaura cross-coupling reaction. *J. Med. Chem.* **2017**, *60*, 1580–1590.
- (16) Hu, Y.; Wang, Y.; Li, F.; Ma, C.; Wang, J. Design and expedient synthesis of organosilanes as potent antivirals targeting multidrug-resistant influenza A viruses. *Eur. J. Med. Chem.* **2017**, *135*, 70–76.
- (17) Li, F.; Ma, C.; Hu, Y.; Wang, Y.; Wang, J. Discovery of potent antivirals against amantadine-resistant influenza A viruses by targeting the M2-S31N proton channel. *ACS Infect. Dis.* **2016**, *2*, 726–733.
- (18) Li, F.; Ma, C.; DeGrado, W. F.; Wang, J. Discovery of highly potent inhibitors targeting the predominant drug-resistant S31N mutant of the influenza A virus M2 proton channel. *J. Med. Chem.* **2016**, *59*, 1207–1216.
- (19) Wang, J.; Wu, Y.; Ma, C.; Fiorin, G.; Wang, J.; Pinto, L. H.; Lamb, R. A.; Klein, M. L.; DeGrado, W. F. Structure and inhibition of the drug-resistant S31N mutant of the M2 ion channel of influenza A virus. *Proc. Natl. Acad. Sci. U. S. A.* **2013**, *110*, 1315–1320.
- (20) Kerns, E.; Di, L. *Drug-like Properties: Concepts, Structure Design and Methods: from ADME to Toxicity Optimization*. Academic Press: Boston, 2016.
- (21) Wanka, L.; Iqbal, K.; Schreiner, P. The lipophilic bullet hits the targets: medicinal chemistry of adamantane derivatives. *Chem. Rev.* **2013**, *113*, 3516–3604.
- (22) Kalgutkar, A. S.; Nguyen, H. T.; Vaz, A. D.; Doan, A.; Dalvie, D. K.; McLeod, D. G.; Murray, J. C. In vitro metabolism studies on the isoxazole ring scission in the anti-inflammatory agent leflunomide to its active alpha-cyanoenol metabolite A771726: mechanistic similarities with the cytochrome P450-catalyzed dehydration of aldoximes. *Drug Metab. Dispos.* **2003**, *31*, 1240–1250.
- (23) Gramec, D.; Peterlin Masic, L.; Sollner Dolenc, M. Bioactivation potential of thiophene-containing drugs. *Chem. Res. Toxicol.* **2014**, *27*, 1344–1358.
- (24) White, J. R. Dipeptidyl peptidase-IV inhibitors: pharmacological profile and clinical use. *Clin Diabetes* **2008**, *26*, 53–57.
- (25) Repetto, G.; del Peso, A.; Zurita, J. L. Neutral red uptake assay for the estimation of cell viability/cytotoxicity. *Nat. Protoc.* **2008**, *3*, 1125–1131.
- (26) Hayden, F. Newer influenza antivirals, biotherapeutics and combinations. *Influenza Other Respir. Viruses* **2013**, *7*, 63–75.
- (27) Huggins, J. W.; Robins, R. K.; Canonico, P. G. Synergistic antiviral effects of ribavirin and the C-nucleoside analogs tiazofurin and selenazofurin against togaviruses, bunyaviruses, and arenaviruses. *Antimicrob. Agents Chemother.* **1984**, *26*, 476–480.
- (28) Meletiadi, J.; Pournaras, S.; Roilides, E.; Walsh, T. J. Defining fractional inhibitory concentration index cutoffs for additive interactions based on self-drug additive combinations, Monte Carlo simulation analysis, and in vitro-in vivo correlation data for antifungal drug combinations against *Aspergillus fumigatus*. *Antimicrob. Agents Chemother.* **2010**, *54*, 602–609.
- (29) Hu, Y.; Zhang, J.; Musharrafieh, R. G.; Ma, C.; Hau, R.; Wang, J. Discovery of dapivirine, a nonnucleoside HIV-1 reverse transcriptase inhibitor, as a broad-spectrum antiviral against both influenza A and B viruses. *Antiviral Res.* **2017**, *145*, 103–113.
- (30) Hu, Y.; Zhang, J.; Musharrafieh, R.; Hau, R.; Ma, C.; Wang, J. Chemical genomics approach leads to the identification of hesperadin, an aurora B kinase inhibitor, as a broad-spectrum influenza antiviral. *Int. J. Mol. Sci.* **2017**, *18*, 1929.
- (31) DiMasi, J. A.; Grabowski, H. G.; Hansen, R. W. Innovation in the pharmaceutical industry: New estimates of R&D costs. *J. Health Econ* **2016**, *47*, 20–33.
- (32) Wang, J.; Ma, C.; Wang, J.; Jo, H.; Canturk, B.; Fiorin, G.; Pinto, L. H.; Lamb, R. A.; Klein, M. L.; DeGrado, W. F. Discovery of novel dual inhibitors of the wild-type and the most prevalent drug-resistant mutant, S31N, of the M2 proton channel from influenza A virus. *J. Med. Chem.* **2013**, *56*, 2804–2812.
- (33) Balannik, V.; Wang, J.; Ohgashi, Y.; Jing, X.; Magavern, E.; Lamb, R. A.; DeGrado, W. F.; Pinto, L. H. Design and pharmacological characterization of inhibitors of amantadine-resistant mutants of the M2 ion channel of influenza A virus. *Biochemistry* **2009**, *48*, 11872–11882.
- (34) Hatakeyama, S.; Sakai-Tagawa, Y.; Kiso, M.; Goto, H.; Kawakami, C.; Mitamura, K.; Sugaya, N.; Suzuki, Y.; Kawaoka, Y. Enhanced expression of an α 2,6-linked sialic acid on MDCK cells improves isolation of human influenza viruses and evaluation of their sensitivity to a neuraminidase inhibitor. *J. Clin. Microbiol.* **2005**, *43*, 4139–4146.